International Journal of Advanced Structural Engineering (2019) 11 (Suppl 1):S19–S34
https://doi.org/10.1007/s40091-019-00252-8

ORIGINAL RESEARCH

Numerical investigation of a new structural configuration of a concrete barrier wall under the effect of blast loads

Ahmed K. Taha[1] · Zhengguo Gao[1] · Dahai Huang[1] · M. S. Zahran[2]

Received: 10 September 2019 / Accepted: 18 November 2019 / Published online: 28 November 2019

Abstract

In this study, a non-linear three-dimensional hydrocode numerical simulation was carried out using AUTODYN-3D, which is an extensive code dealing with explosion problems. A high explosive material (comp-B) is blasted against several concrete wall barriers. The model was first validated using referenced experimental tests and has shown good results. Several numerical models were carried out to study the effect of changing the shape of wall barrier from flat to convex curve and concave curve, and also investigated the effect of changing the angle of curvature. The results showed that changing the shape of a wall barrier from flat to convex curve has the best performance in mitigating the effect of blast waves. It is also concluded that convex walls with 60° angle of curvature have the best performance compared to other barrier walls.

Keywords Concrete · Explosion · Composition B · Wall barrier · Numerical simulation · Blast wave

Introduction

With the increasing threat of terrorism and the rapid development of technology, the probability of accidental explosions such as incident blasts, mine explosions, and terrorist attacks has increased; protecting important structures against explosive impacts has become a great concern (Goel and Matsagar 2013; Hetherington and Smith 2014; Hinman and Engineers 2011; Li et al. 2009; Remennikov and Rose 2007; Wang et al. 2013; Wu 2012; Wu et al. 2010; Zhou and Hao 2008).

Blast waves are formed by detonating explosives in the open field, during detonation, a very large amount of energy and pressure are released in a very small fraction of time due to the decomposition of explosives into gases, as shown in Fig. 1. The pressure of the emitted gases ranges from 10 to 30 GPa and temperature ranges from 3000 to 4000 c. If the solid material is directly in contact with the explosive, a shock wave is generated in the material, while a blast wave is generated if the explosion happens in air medium (Ben-Dor et al. 2000; Sandhu et al. 2017).

The intensive pressure of these explosions causes critical damage to the nearby buildings and human beings in the perimeter of the explosion (Alsubaei 2015; Baker et al. 2012; Berger et al. 2015). To reduce the losses of lives and building resources, protecting structures against blast load is studied extensively with different techniques or methods. One of these techniques is using different sizes and shapes of Barriers to diffract the blast wave, leaving behind it a complex flow field that changes the load exerted on the target (Aghdamy et al. 2013; Luccioni and Ambrosini 2010; Tiwari et al. 2016; Xia et al. 2014).

Numerous researchers have studied the effects of shock waves on different geometric configurations theoretically, numerically, and experimentally (Azmi et al. 2019; Chaudhuri et al. 2013; Igra et al. 2001; Lu et al. 2005; Nam et al. 2016; Nurick et al. 1996, 2006; Smith et al. 1999). Such as, Rouse (2010) studied the mitigating effects of a blast

✉ Ahmed K. Taha
ahmedtaha@buaa.edu.cn

Zhengguo Gao
gaozg@buaa.edu.cn

Dahai Huang
huangdh@buaa.edu.cn

M. S. Zahran
m.s.zahran@mtc.edu.eg

[1] School of Transportation Science and Engineering, Beihang University (Beijing University of Aeronautics and Astronautics), Beijing 100191, People's Republic of China

[2] Department of Civil Engineering, Military Technical College, cairo, Egypt

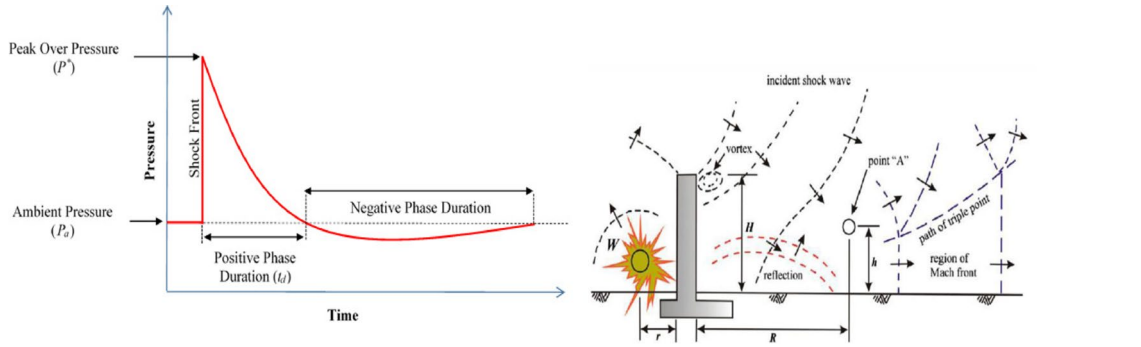

(a) Ideal free field blast wave profile (Inderpal Singh Sanhu, 2017)

(b) The effect of blast waves on barrier wall (alsubaei, 2015)

Fig. 1 Blast wave effects

barrier wall. This study used a scaling method to make an experimental research on the effect of the barrier wall in reducing the effect of the pressure wave on the area behind the barrier. Two parameters were studied in this research: the barrier height and the standoff distance where the study used 73 grams of hemi-spherical-shaped C4 explosive charges on a barrier wall.

Berger et al. (2015) investigated experimentally and numerically using different barrier configurations to attenuate the shock wave effects. The experiments were performed in a shock tube equipped with a high-speed camera. Aghdamy et al. (2013) investigated numerically the effect of retrofitting masonry walls subjected to blast with nano-particle reinforced polymer and aluminum foam numerical models were validated using available test data. Different pressures and impulses were applied on the retrofitted walls and their efficiency was investigated. Xia et al. (2014) performed a numerical investigation on reinforced concrete cladded with metallic foam using LS-dyna. The model was validated using field blast testing.

Parametric studies were conducted to investigate the effect of the thickness of the reinforced concrete members and the different properties of foam. Due to the development in the engineering technologies, researchers/designers developed a new way of thinking to solve the daily life problems. Recently, numerous researchers have concluded that the inspiration from nature (Biomimicry) is the optimum solution to solve the most sophisticated engineering problems (Rong and Thong 2015).

Bio-inspired technique is an approach to solve the human challenges through studying the natures' designs and then imitate/mimic them to seek sustainable solutions (Wilson 2008). Since, the current work discusses the protection/armor systems, several investigations have been carried out to study the armor mechanisms, protection systems, ballistics armor, and flexible armor; for instance, the multifunctional shell of chitons. The shell consists of two completely different segmented armors, central plates, and peripheral scales, which are seamlessly integrated together in one system. The plates and scales differ in size, degrees of freedom, and level of protection (Connors 2014). Another example is that the seahorse tail is composed of subdermal bony plates arranged in articulating ring-like segments that overlap for controlled ventral bending and twisting (Porter et al. 2013). The bony plates are highly deformable materials designed to slide past one another and buckle when compressed. This complex plate and segment motion, along with the unique hardness distribution and structural hierarchy of each plate, provide seahorses with joint flexibility while shielding them against impact and crushing.

Based on the aforementioned literature review, it is concluded that there are different techniques that can be used to mitigate the effect of shock waves. The shape configuration of the concrete barrier wall is modified from the ordinary flat barrier wall to curved barrier wall mimicking the protecting shield of the turtle and armadillo where their curved shield protects them from the various attacks of enemies and it provides these animals with the maximum protection it can offer according to its characteristics. Their shield could have a lot of shapes to protect them but nature gave them the curved shape, so we thought that this shape is the best protection for them, so we could benefit from this shape in protection from various loads (in our case blast loads).

Therefore, the current study proposes a new configuration of protected wall to deviate, absorb, and reflect the blast waves. The idea of the new proposed protected wall is inspired from the engineering Biomimicry, such as the armadillo, the turtle which use their curved geometric shapes to act as an optimized natural armor, as shown in Fig. 2.

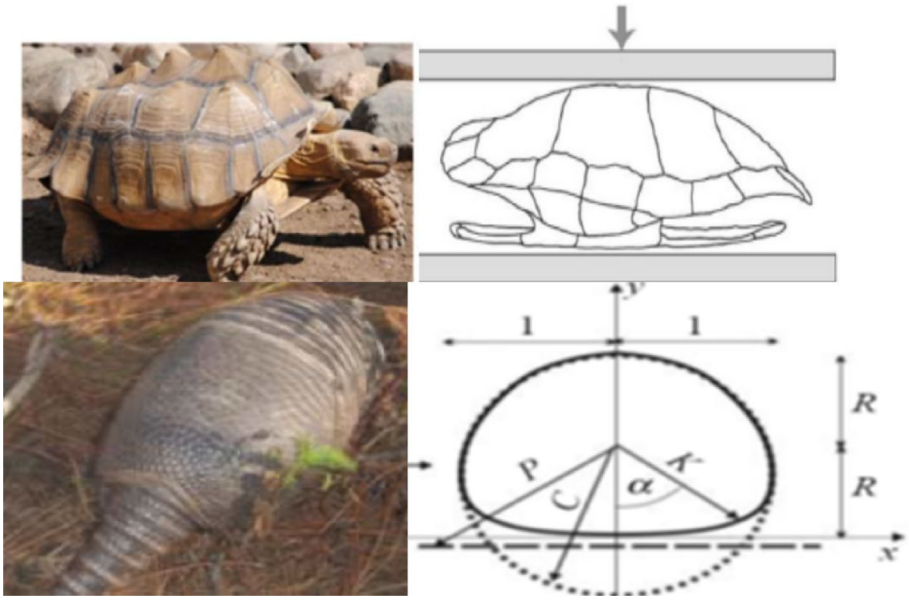

Fig. 2 Turtle and armadillo's curved geometric shape

Therefore, the new proposed protected wall is based on these natural facts. Numerical analysis is performed to simulate the effect of the explosion on the new proposed and traditional configuration of a concrete barrier wall using finite-element software AUTODYN-3D (Autodyn 2005). The finite-element model is validated by available published experimental tests (Hajek et al. 2016). Then, the effect of the geometrical shape of a wall barrier is studied as a comparison is made between flat and curved wall with different angles of curvature to achieve the best performance in the mitigation of the blast wave resulting from the detonation.

Numerical simulations

Numerical simulations are an important means of studying the effect of explosion and blast effects on different structures as conducting experimental investigations is very expensive and needs a lot of equipment and precautions during execution.

Numerical tool: hydrocode

A computer program that is capable of computing strains, stresses, velocities, and propagation of shock waves as a function of time and position is known as a hydrocode. In this study, the hydrocode simulations on the explosion effect on a concrete target are performed using AUTODYN-3D (Mizukaki 2007). In AUTODYN-3D, the fundamental equations together with the initial and boundary conditions are solved using a finite-difference scheme.

Model validation

This paper presents a 3D hydrocode simulation using AUTODYN-3D (Autodyn 2005) on the effect of explosion on a barrier wall target. The experimental data published by Hajek et al. (2016) for two tests carried out using a 500 g explosive are used for validation.

Two experimental tests were used for validation; in the first test, the air domain is modeled with 812,500 elements and 847,926 nodes, and the pressure was measured at standoff distance 6 m from the TNT charge as a typical free-field detonation, as shown in Fig. 3. The results of the numerical simulation compared to the experimental test are as shown in Fig. 4 where the pressure recorded in the experimental test is 22 kPa, while the pressure measured from the numerical model is 22.5 kPa (after excluding the atmospheric pressure which is measured in the numerical simulation in contrary to the experimental test) with a percentage of error of 2.2%.

In the second test, the flat concrete target is modeled with 45,000 element, while for the air domain, it is modeled with 542,488 elements and 566,631 nodes; the pressure was measured at the same standoff distance as the first test (6 m) from the charge, as shown in Fig. 5 but with the presence of a concrete barrier at a distance 5 m from the detonation point. Figure 6 shows the numerical model simulation for the experimental test as described by Hajek et al. (2016).

The height of the barrier is 1.2 m, its width is 3 m, and the thickness is 10 cm, and the compressive strength of concrete used is 156 MPa. The pressure is measured at height 1.2 m from the ground level. The results of the pressure at the gauge point in the numerical test are compared to the results measured in the experimental test, as shown in Fig. 7 where the pressure recorded in the experimental

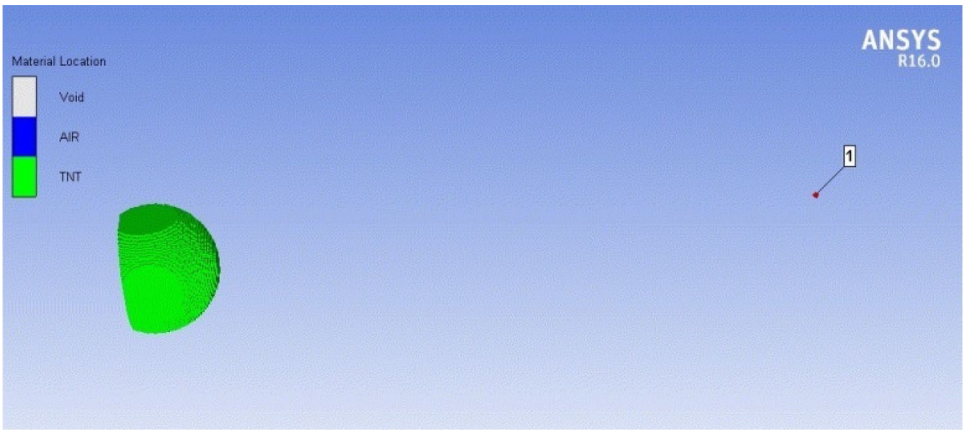

Fig. 3 The numerical model used for validation for the first test

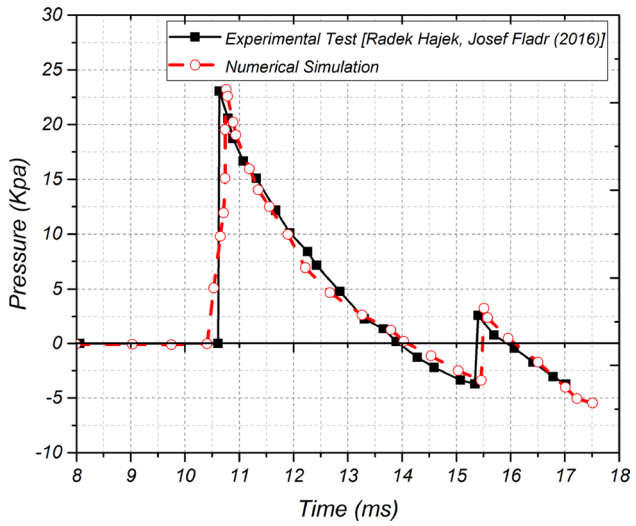

Fig. 4 The pressure measured from the experimental test and the numerical simulation of free-field explosion

test is 9 kPa, while the pressure measured from the numerical model is 9.2 kPa (after excluding the atmospheric pressure which is measured in the numerical simulation in contrary to the experimental test) with a percentage of error of 2.2%.

Proposed structural configuration

The proposed structural configuration is a structural wall at a distance 2 m from an explosive charge of 10 kg TNT and surrounded with air as shown in Fig. 8. For the sake of validation, we have compared the results of a free-field blast of 10 kg TNT at a distance of 2 m from our numerical model where the pressure was 956 kPa, the result of the same blast conditions calculated from TM5 was 930 kPa, while the result calculated from CONWEP was 1102 kPa.

The dimensions of the proposed configuration are as shown in Fig. 9 where three geometrical shapes are proposed: traditional flat barrier wall (TFBW), curved concave wall (CCVW), and curved convex wall (CCXW).

The curved barrier wall is placed in two positions, the first one the side facing the blast wave is the convex side, while the second one the side facing the blast wave is the concave side with different angles of curvature Ø (50°, 60°, and 70°) which are subjected to the detonation of a 10 kg comp-B detonated at a distance 2 m from the barrier wall (Yusof et al. 2014) to detect the geometrical shape which gives the best performance in the mitigation of the blast wave resulting from the detonation.

Seven structural configurations are considered for this study named TFBW, CCVW-70, CCVW-60 and CCVW-50, CCXW-70, CCXW-60, and CCXW-50. For the sake

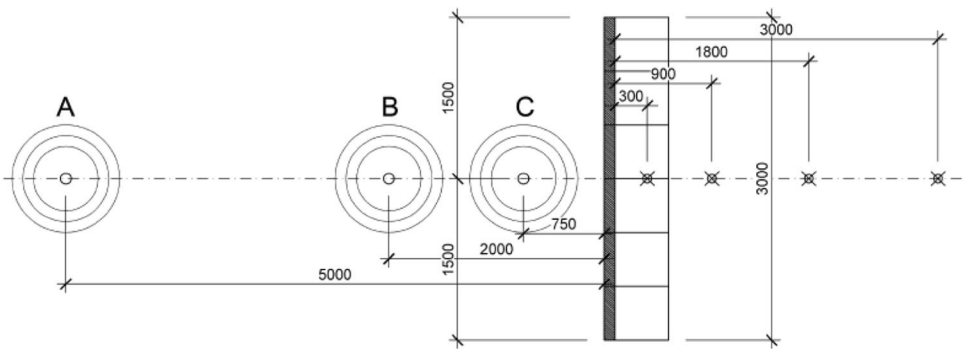

Fig. 5 The field setup for the experimental test (Hajek et al. 2016)

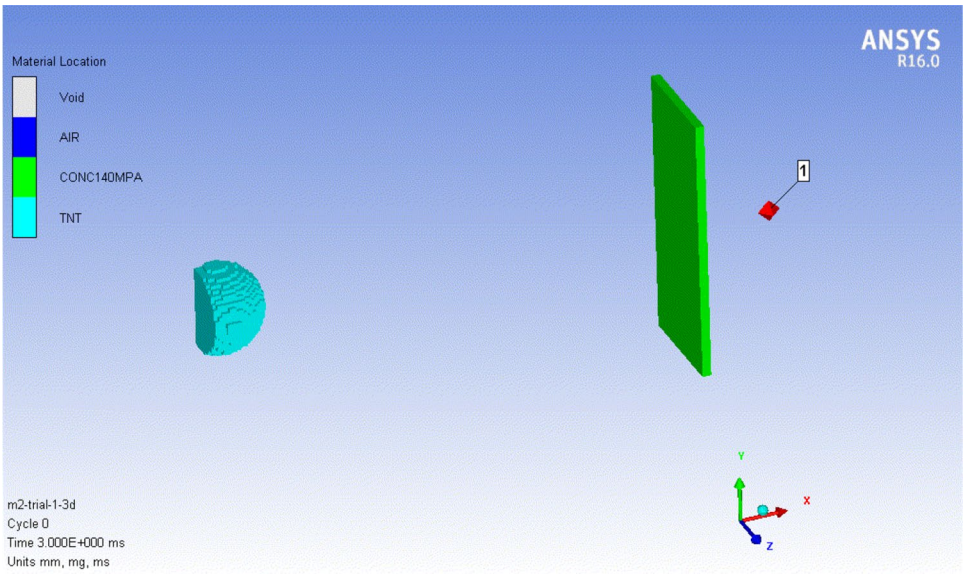

Fig. 6 The numerical model used for validation

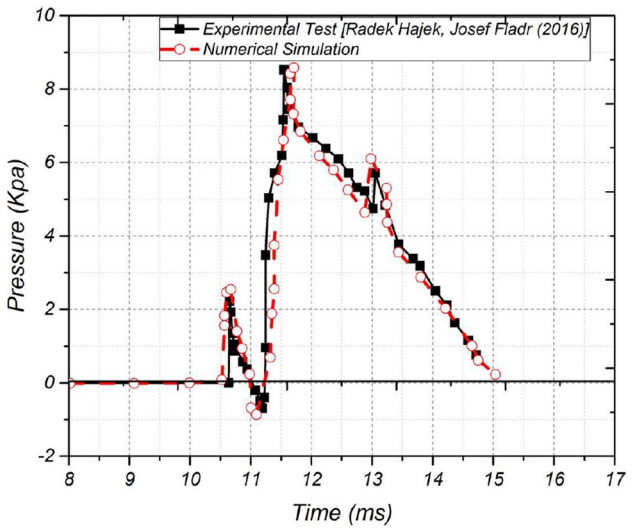

Fig. 7 The pressure measured from the experimental test and the numerical simulation of explosion in the presence of a concrete barrier

of comparison, all the compared configurations have the same weight and height. The TFBW is of height 3000 mm, width 500 mm, and thickness 473 mm, as shown in Fig. 10a, while the CCVW and CCXW are of height 3000 mm, width 500 mm, and variable thicknesses, as shown in Fig. 10b–g.

Finite-element model

In this model, the flat concrete target is modeled with 1960 element, while for the curved concrete target, it is modeled with 1400 element and the air domain is modeled with 1,215,555 elements and 1,254,400 nodes, as shown in Fig. 11. The concrete used in the barrier wall has a compressive strength of 35 MPa. The properties of the used materials are shown in Table 1 (Riedel et al. 1999, 2009; Rogers and Mayhew 1995).

Remap technique was used during numerical simulation (Autodyn 2005). The initial detonation and blast wave propagation of the explosive in free air are first calculated in a 2D domain; the result was then remapped into a 3D space. This technique is used to save time and make the model more efficient.

Flow-out boundary conditions were applied on the outer surfaces of the air domain to allow the pressure of the blast to be dissipated outside the air domain without reflecting and affecting the concrete target. Free-end boundary conditions were applied on the concrete barrier wall on the upper and lower sides, as shown in Fig. 12.

The concrete target is described with the Lagrange solver. Composition B is modeled using Jones–Wilkins–Lee equation of state which models the pressure generated by chemical energy in an explosion. Air was modeled by an ideal gas equation of state, which is one of the simplest forms of equation of state.

Numerical results and analysis

This section presents and discusses the results of different pressure gauges placed in different locations on the concrete barrier wall and behind it, as shown in Fig. 13, to show the effect of different shapes and angles of curvature of the wall barrier, while Table 2 presents the peak pressure recorded for each gauge for the studied models. The pressure vs. time history is investigated at each gauge to evaluate the peak pressure at the proposed models. Also, the effect of the wall barrier on the pressure behind the wall is also investigated by

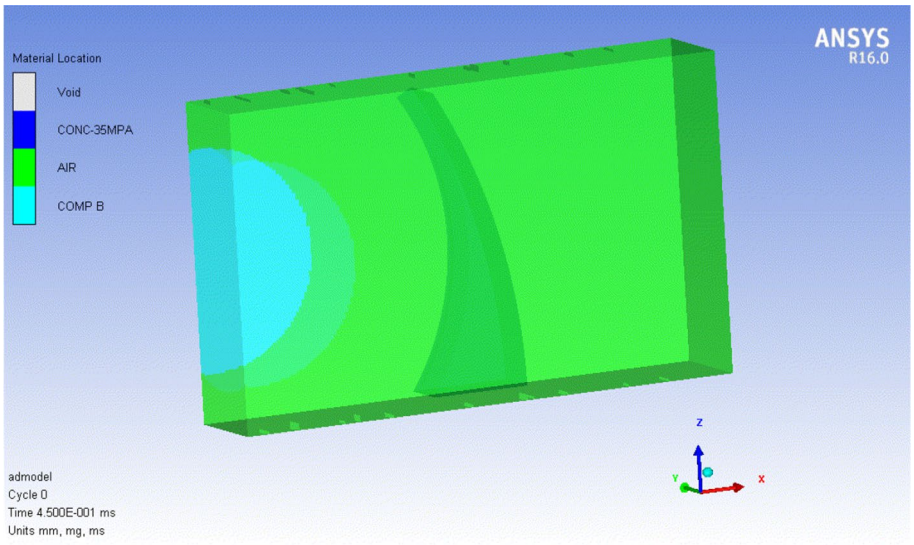

Fig. 8 Proposed numerical model

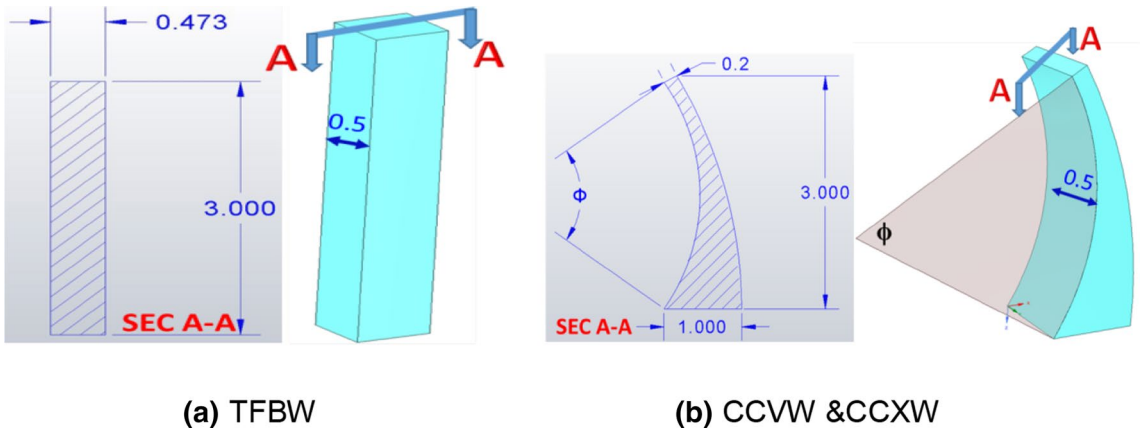

Fig. 9 Dimensions of concrete barrier wall

evaluating the pressure at gauge 7. Also, the internal energy inside the concrete barrier is demonstrated.

Over-pressure

Gauge 1 is in the front lower part of the concrete barrier. As shown in Fig. 14 for the concave walls, the results of pressure measured on this gauge show different responses of different barrier shapes and configurations on the pressure measured in this location as we see that when comparing the pressure measured at gauge 1 for TFBW, and for CCVW-60, the pressure measured at CCVW-60 is slightly lower (232 kPa) than that measured at TFBW which is 233 kPa, while when the angle of curvature (Ø) was 50° in the model CCVW-50, the pressure increased to 365 kPa, and when the angle of curvature (Ø) increased to 70° in the model CCVW-70, the pressure increased dramatically to 1334 kPa.

Gauge 2 is in the front middle part of the concrete barrier. As shown in Fig. 14, the results of pressure measured on this gauge show different responses of different barrier shapes and configurations on the pressure measured in this location as the pressure measured in the model TFBW is the highest and it decreases slightly in model CCVW70 (2151 kPa). When the angle of curvature (Ø) of the wall decreased to 60° (model CCVW60), the pressure decreased to 1676 kPa, and then, the pressure decreased much more to 1332 kPa when the angle of curvature (Ø) decreased to 50° (CCVW50).

While for the convex walls, as shown in Fig. 15, the pressure measured at gauge 1 for CCXW-60 (110 kPa) is a lot lower than that measured at TFBW, while when the angle of curvature (Ø) was 50° in the model CCXW-50, the pressure increased to 446 kPa, and when the angle of curvature (Ø) increased to 70° in the model CCXW-70, the pressure increased dramatically to 799 kPa.

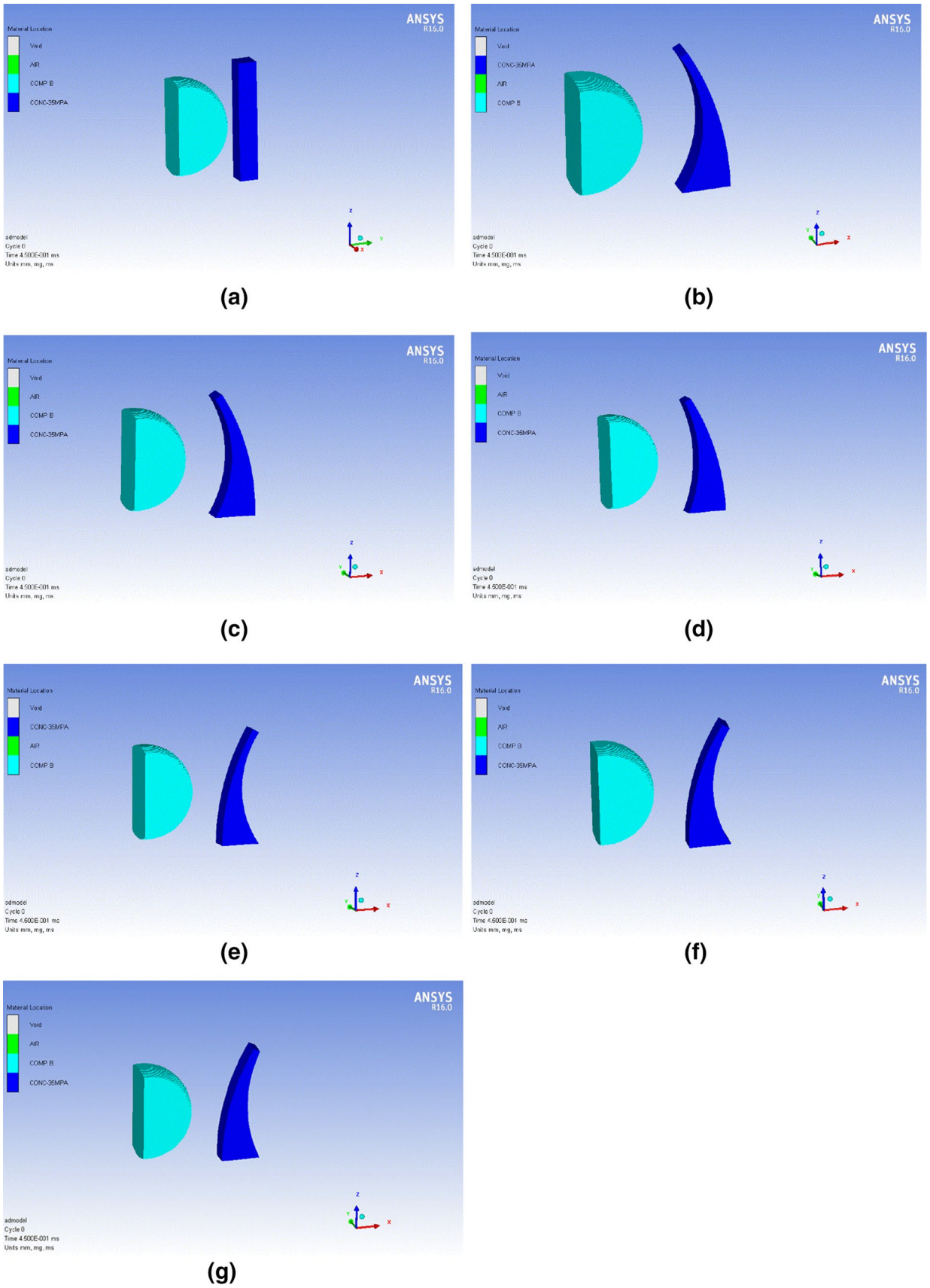

Fig. 10 Structural configuration of the proposed model. **a** TFBW, **b** CCVW-70, **c** CCXW-60, **d** CCVW-50, **e** CCXW-70, **f** CCXW-60, **g** CCXW-50

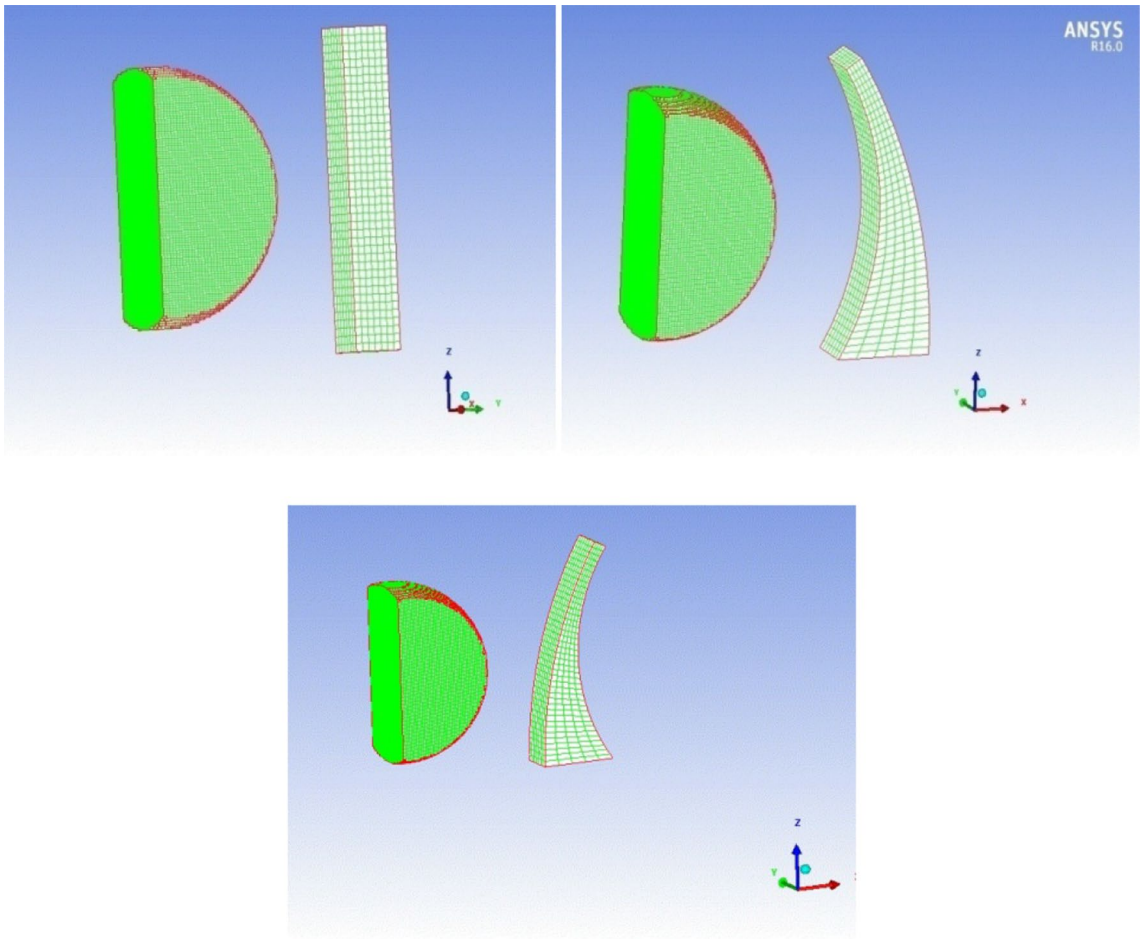

Fig. 11 Elements of the proposed TFBW, CCVW, and CCXW models

Table 1 Properties of used materials

Material	Equation of state	Strength model	Reference density (kg/m^3)	Shear modulus (GPa)	References
Concrete	P-alpha	RHT	2750	16.7	Riedel and Kawai (2009) and Riedel et al. (1999)
Comp. B	JWL	–	1710	–	
Air	Ideal gas	–	1.225	–	Rogers and Mayhew (1995)

For gauge 2 as shown in Fig. 15, the pressure measured for the model CCXW-70 is 2169 kPa. When the angle of curvature (Ø) of the wall decreased to 60° (model CCXW-60), the pressure decreased to 428 kPa, and then, the pressure increased again to 1410 kPa when the angle of curvature (Ø) decreased to 50° (CCXW-50).

Gauge 3 is in the front upper part of the concrete barrier. As shown in Fig. 16, the results of pressure measured on this gauge show different responses of different barrier shapes and configurations on the pressure measured in this location as the pressure measured on the TFBW is lower (233 kPa) than the pressure measured on the model CCVW-70 (1139 kPa). However, when the angle of curvature (Ø) decreased to 60° (model CCVW-60), the pressure decreased to 356 kPa, and then, it decreased more to 223 kPa when the angle of curvature (Ø) decreased to 50° in model CCVW-50 to lower than the value of the model TFBW.

Gauge 4 is in the lower back part of the concrete barrier in the back face. As shown in Fig. 16, the results of pressure measured on this gauge show different responses of different barrier shapes and configurations on the pressure measured in this location as the pressure measured in the model TFBW is higher (870 kPa) than the pressure measured in the model CCVW-70 (698 kPa), and when the angle of curvature (Ø)

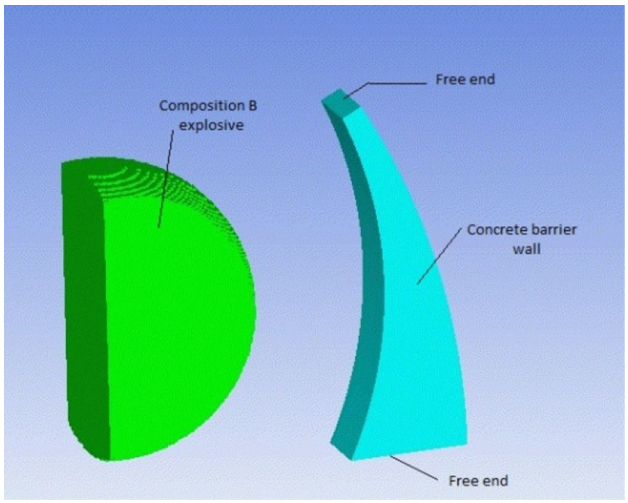

Fig. 12 FEM boundary conditions of the concrete barrier wall

decreased to 60° in model CCVW-60, the pressure decreased to 306 kPa, and then, it decreased more to 293 kPa when the angle of curvature (Ø) decreased to 50° in model CCVW-50.

While for the convex wall, as shown in Fig. 17 for gauge 3, the pressure measured on the model CCXW-70 is 1098 kPa. However, when the angle of curvature (Ø) decreased to 60° (model CCXW-60), the pressure decreased to 460 kPa, and then, it decreased more to 104 kPa when the angle of curvature (Ø) decreased to 50° in model CCXW-50 which is the lowest pressure for all models.

However, for gauge 4, as shown in Fig. 17, the pressure measured in the model CCXW-70 is 389 kPa, and when the angle of curvature (Ø) decreased to 60° in model CCXW-60, the pressure decreased to 142 kPa, and then, it increased again to 379 kPa when the angle of curvature (Ø) decreased to 50° in model CCXW-50.

Gauge 5 is in the middle back part of the concrete barrier in the back face. As shown in Fig. 18 for concave walls, the results of pressure measured on this gauge show different responses of different barrier shapes and configurations on the pressure measured in this location as the pressure measured in the model TFBW is 1497 kPa which is lower than the pressure measured on the curved wall in the model CCVW-70 (3355 kPa). However, when the angle of curvature (Ø) decreased to 60° in the model CCVW-60, the pressure decreased to 1335 kPa, and then, it increased once again to 1591 kPa when the angle of curvature (Ø) decreased to 50° in the model CCVW-50.

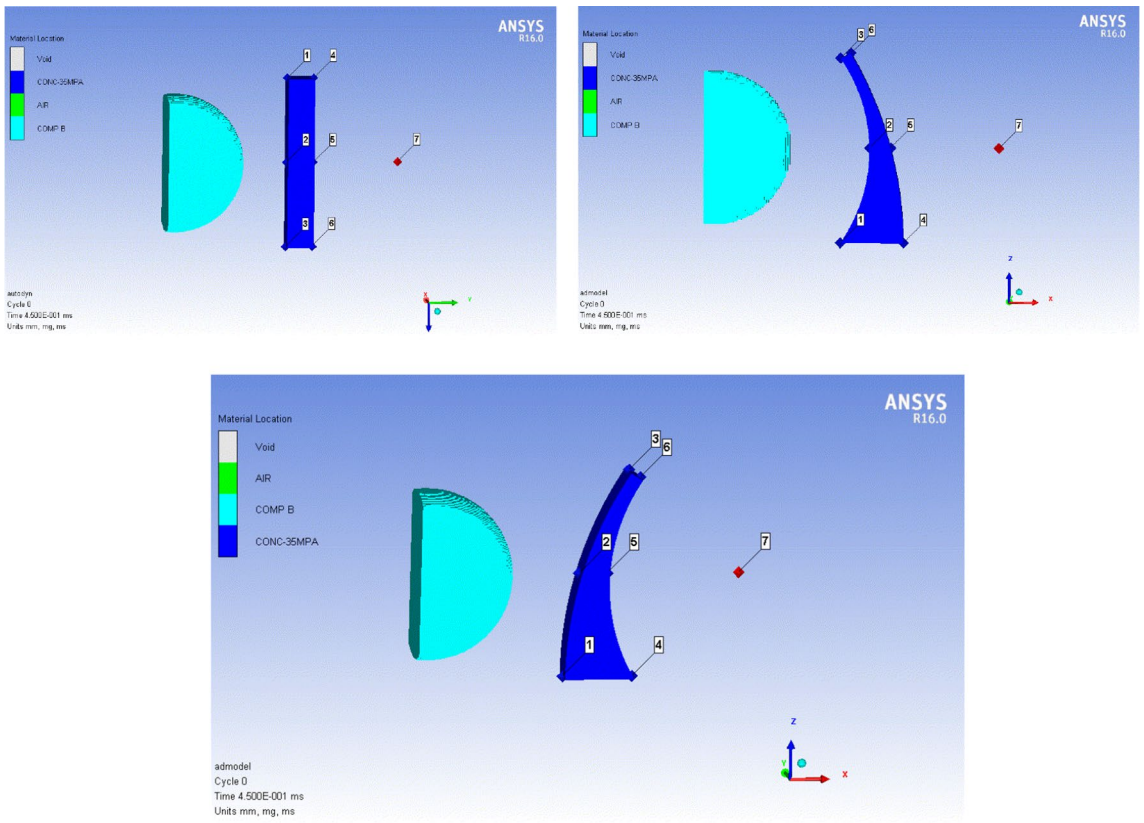

Fig. 13 Locations of added gauges

Table 2 Peak pressure for gauges

Model	TFBW	CCVW-70	CCVW-60	CCVW-50	CCXW-70	CCXW-60	CCXW-50
Gauge no.	Peak pressure (kPa)						
1	233	1334	232	365	799	110	446
2	2203	2151	1676	1332	2169	428	1410
3	233	1139	356	223	1098	460	104
4	870	698	306	293	389	142	379
5	1497	3355	1335	1591	1666	1038	1401
6	870	202	378	550	304	146	578
7	282	308	162	234	308	124	237

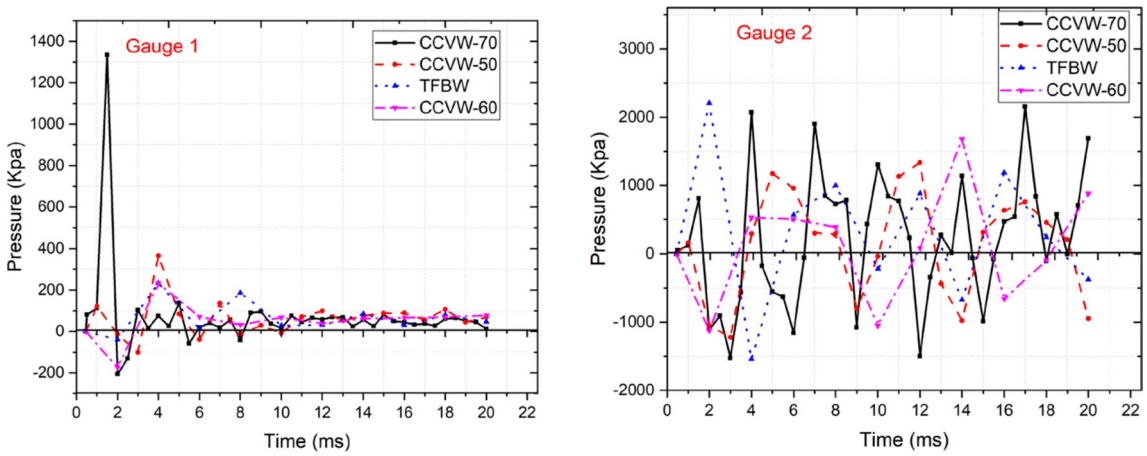

Fig. 14 Pressure–time history of gauge 1 and gauge 2 for concave walls

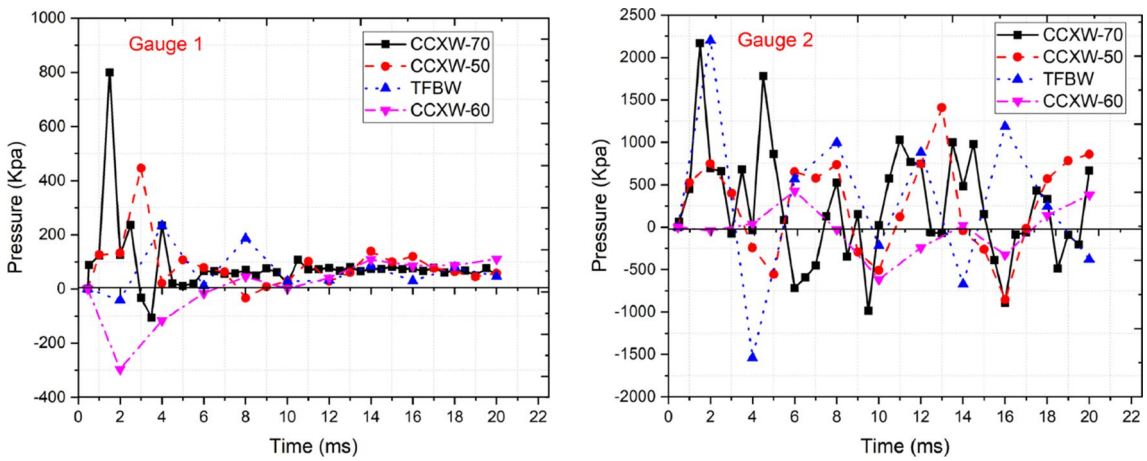

Fig. 15 Pressure–time history of gauge 1 and gauge 2 for convex walls

Gauge 6 is in the upper back part of the concrete barrier in the back face. As shown in Fig. 18, the results of pressure measured on this gauge show different responses of different barrier shapes and configurations on the pressure measured in this location as the pressure measured on the flat wall in the model TFBW is 870 which is higher than the pressure measured in the model CCVW-70 (202 kPa).

However, when the angle of curvature (Ø) decreased to 60° in the model CCVW-60, the pressure increased to 378 kPa, and then, it increased once again to 550 kPa when the angle of curvature (Ø) decreased to 50° in the model CCVW-50.

While for the convex walls, as shown in Fig. 19, the pressure measured in gauge 5 in the model CCXW-70

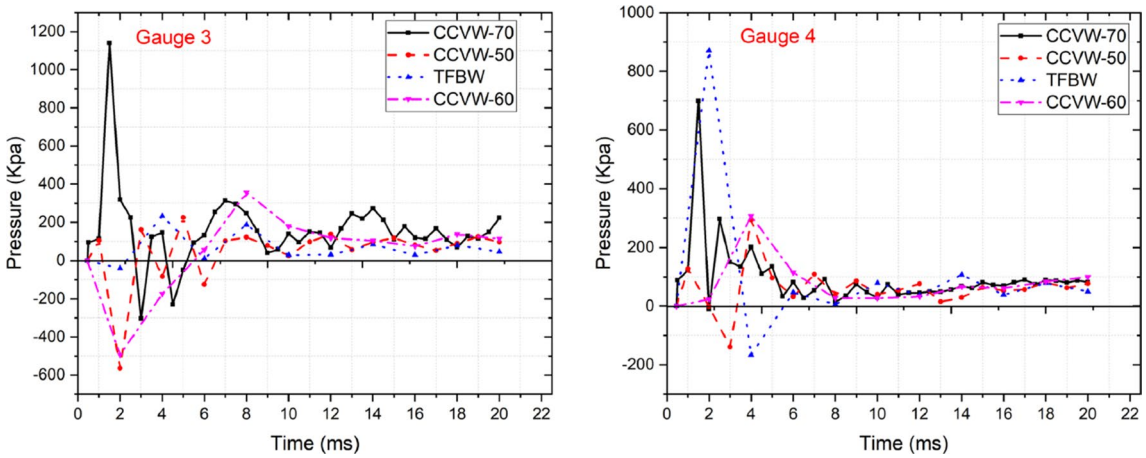

Fig. 16 Pressure–time history of gauge 3 and gauge 4 for concave walls

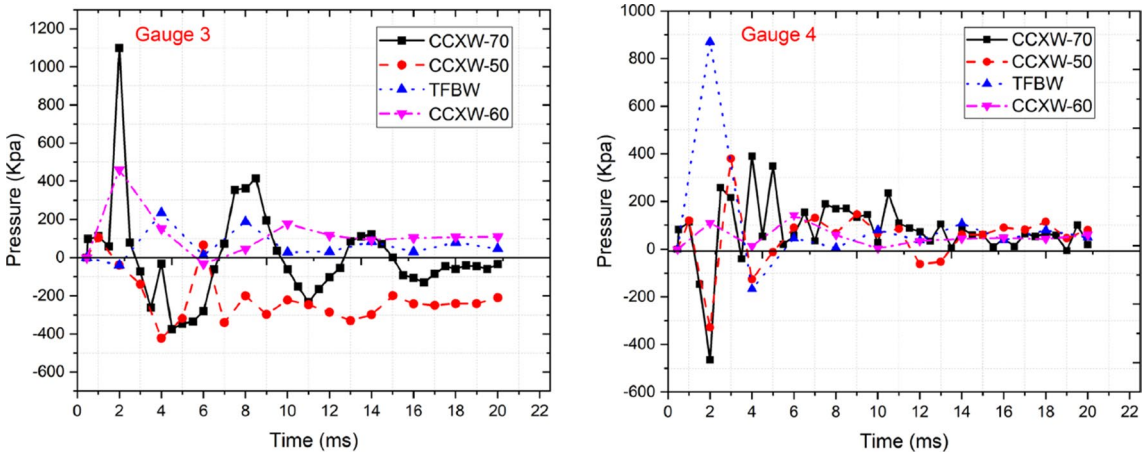

Fig. 17 Pressure–time history of gauge 3 and gauge 4 for convex walls

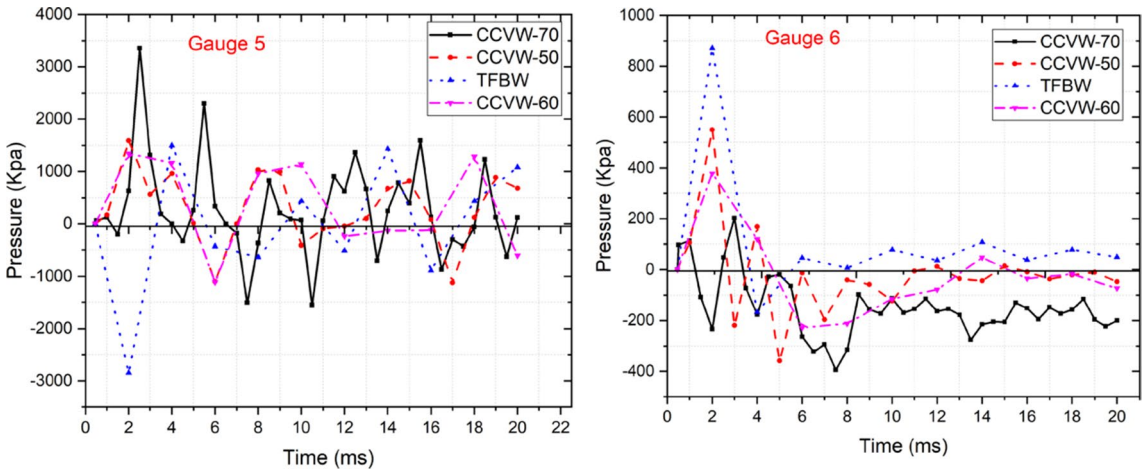

Fig. 18 Pressure–time history of gauge 5 and gauge 6 for concave walls

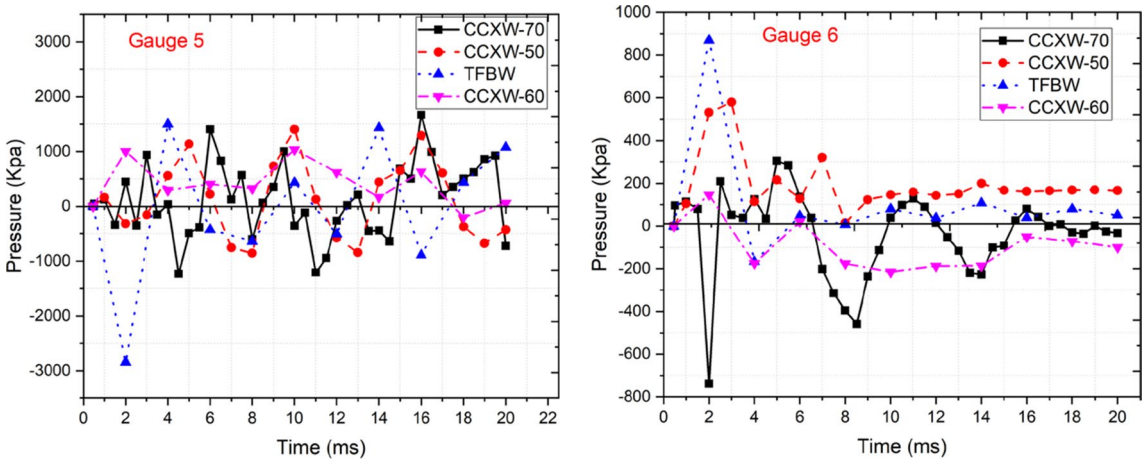

Fig. 19 Pressure–time histories of gauge 5 and gauge 6 for convex walls

is 1666 kPa. However, when the angle of curvature (Ø) decreased to 60° in the model CCXW-60, the pressure decreased to 428 kPa, and then, it increased once again to 1401 kPa when the angle of curvature (Ø) decreased to 50° in the model CCXW-50.

While for gauge 6, as shown in Fig. 19, pressure measured in the model CCXW-70 is 304 kPa, but when the angle of curvature (Ø) decreased to 60° in the model CCXW-60, the pressure increased to 460 kPa, and then it increased once again to 578 kPa when the angle of curvature (Ø) decreased to 50° in the model CCXW-50.

Gauge 7 is at a distance 1.5 m behind the concrete barrier and this gauge shows the variation of the effect of the explosion on any object or any living organisms behind the barrier. As shown in Fig. 20, the pressure measured on the flat wall in the model TFBW has a high value (282 kPa); then, the pressure increased in the model CCVW-70 to 308 kPa and when the angle of curvature (Ø) decreased to 60° in the model CCVW-60 the pressure decreased to 162 kPa, and then, it increased to 234 kPa when the angle of curvature (Ø) decreased to 50° in the model CCVW-50.

While for the convex wall, as shown in Fig. 21 in the model CCXW-70, the pressure is 308 kPa and when the angle of curvature (Ø) decreased to 60° in the model CCXW-60, the pressure decreased to 156 kPa, and then, it increased to 237 kPa when the angle of curvature (Ø) decreased to 50° in the model CCXW-50.

As an example, it can be observed from Table 1 and Fig. 22 that the max pressure at gauge 7 (located at 1.5 m behind the wall barrier) has its maximum value (308 kPa) for the model CCVW-70 where the figure shows the least area of the barrier wall affected by the blast wave and then as the area of the barrier wall affected by the blast wave increases, the pressure recorded at gauge 7 decreases as it

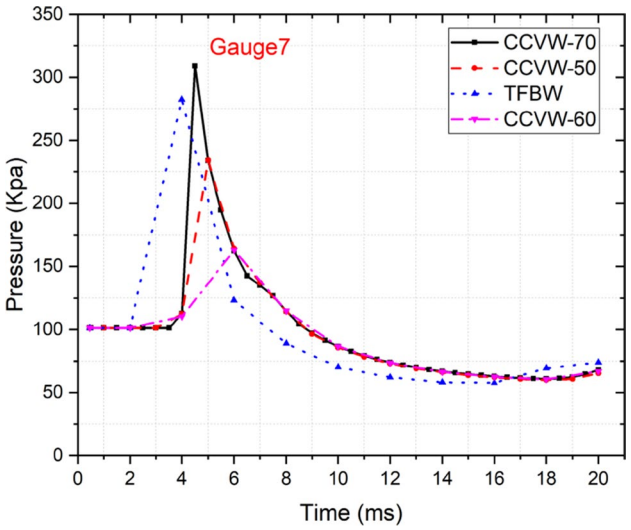

Fig. 20 Pressure–time history of gauge 7 for concave walls

reaches 162 kPa in the model CCXW-60 with a percentage of decrease of 47.4%. Therefore, we can conclude that the greater the energy absorbed by the wall, the lower the pressure is behind the wall.

Internal energy

The internal energy inside the concrete barrier wall is evaluated and demonstrated in the following section, as shown in Fig. 23. Where the concrete barrier wall CCVW-70 has the least internal energy ($8.45e^{7}$μj), while the concrete barrier wall CCXW-60 has the highest internal energy ($1.486e^{8}$ μj).

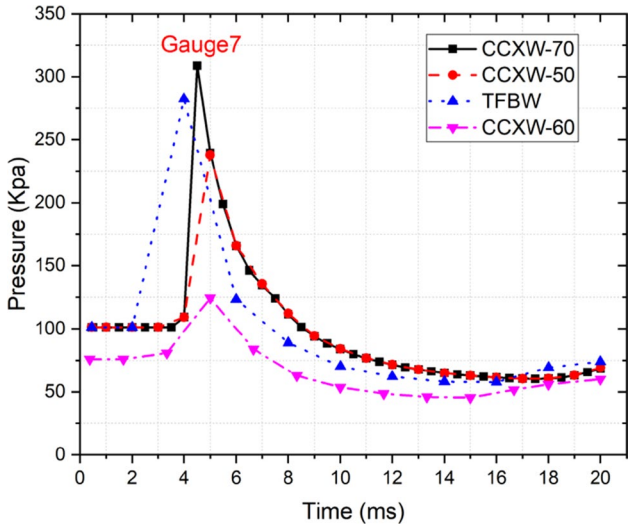

Fig. 21 Pressure–time history of gauge 7 for convex walls

Discussion

As observed from the pressure results from different gauges and Fig. 24 that curved walls have better performance in blast resistance than flat walls. When analyzing the results of pressure gauges to compare between flat and concave walls, we can see that for the near side facing the detonation wave, the middle portion of the flat wall experiences more pressure than the concave wall, while for the upper and lower portion, the concave wall experiences more pressure as the reflected waves in the concave wall cause it to experience more pressure than of the flat wall. For the distant face, the pressure in the middle portion of the concave wall is higher than the flat wall due to the shape of the concave wall which allows the pressure wave to slide easier than the flat wall, while the pressure for the upper and lower portion for the concave wall is lower than the flat one.

When comparing the results of the concave and the convex wall, we can conclude that for the near side facing the detonation wave, the pressure values have no great difference for the middle portion, while for the upper and lower portion, the values are remarkably lower for the convex wall

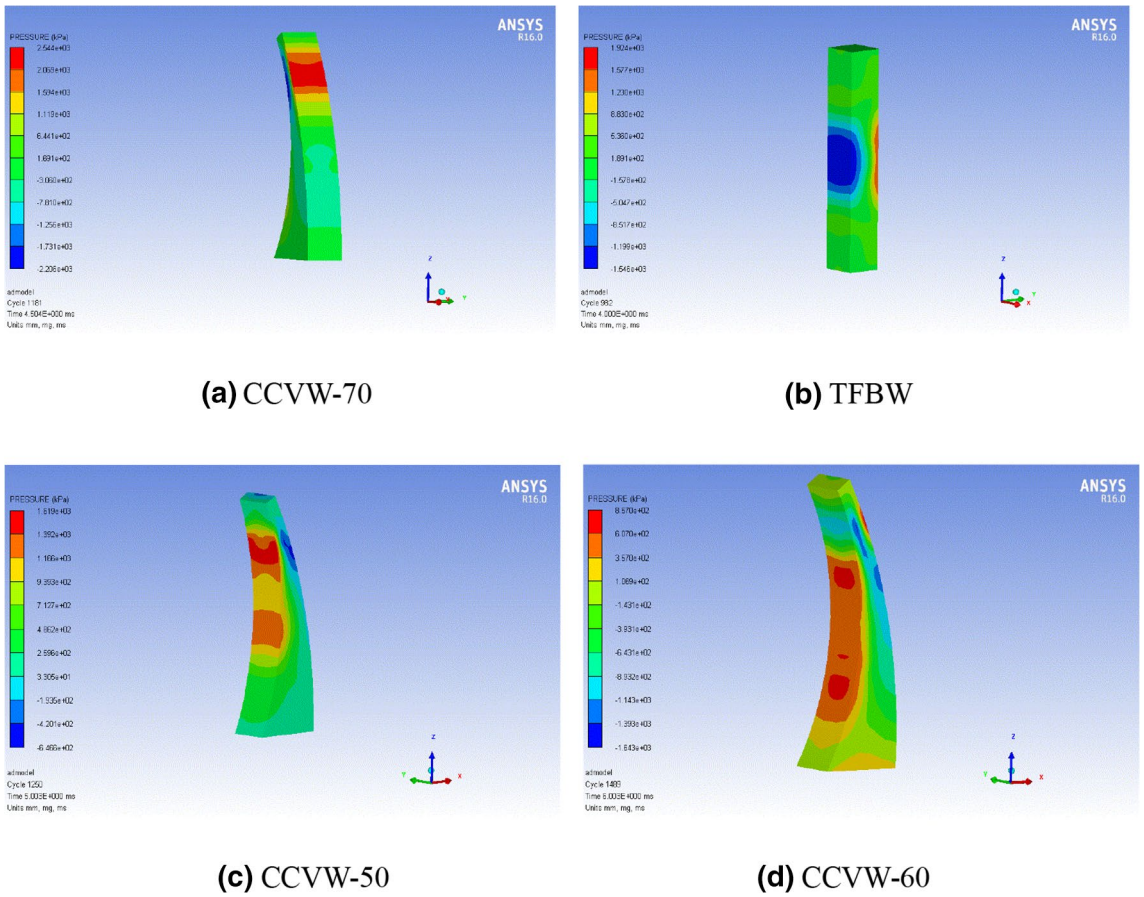

Fig. 22 Area of the concrete barrier wall affected by pressure

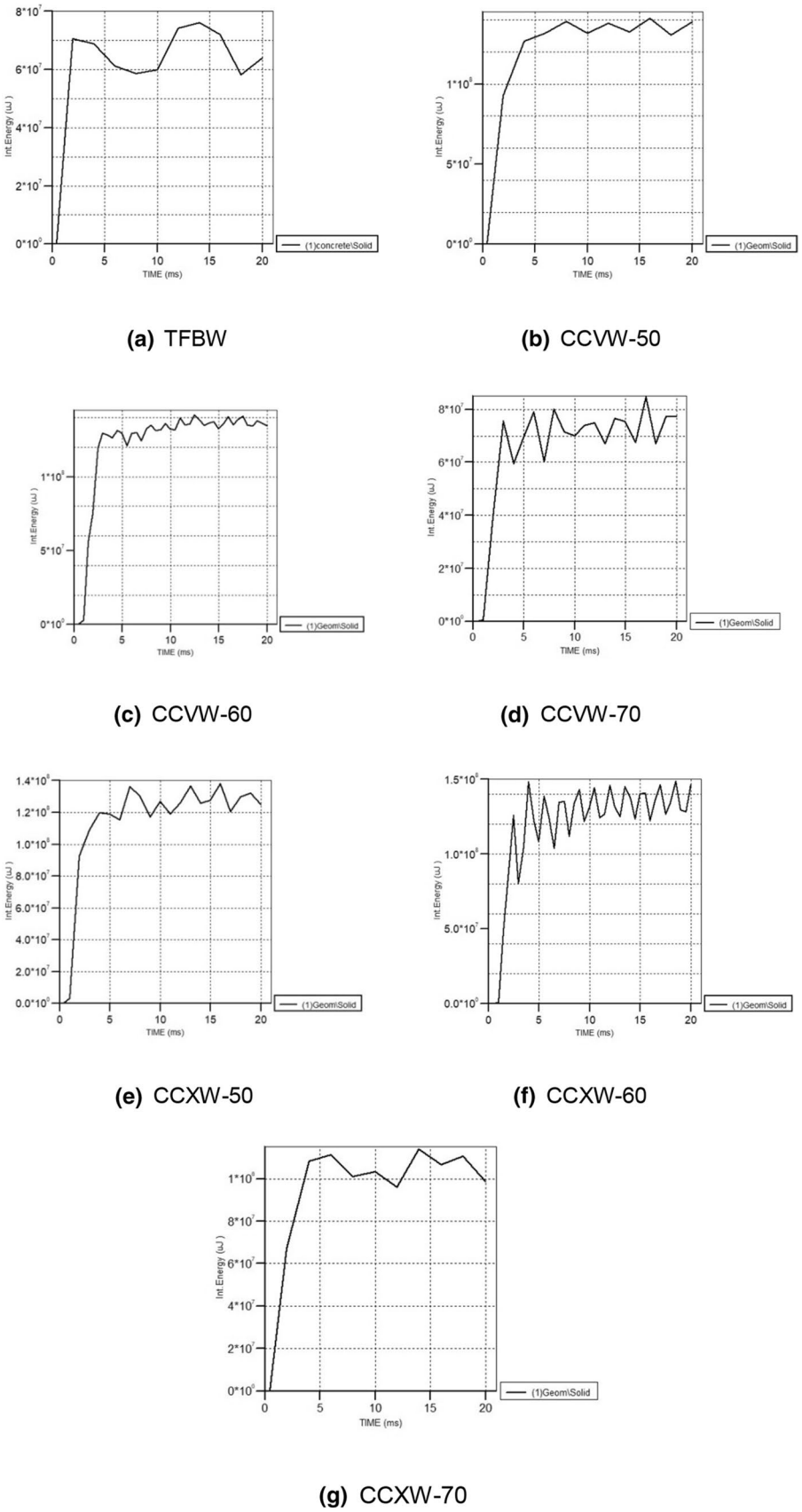

Fig. 23 Internal energy of concrete barrier wall for different models

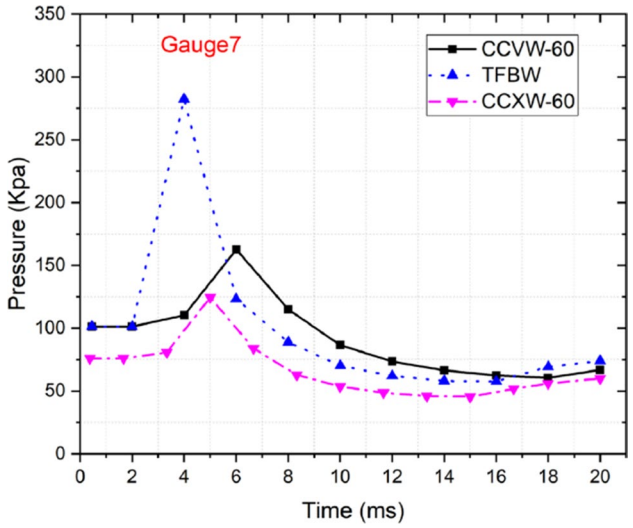

Fig. 24 Pressure–time history of gauge 7 for flat and curved walls

than the concave wall, the cause of this is the reflected waves as when the incident wave impacts the convex wall, it diffracts away from the wall in the upper and lower direction, while for the concave wall, it reflects them in the direction of the upper and lower portion which causes the pressure to go high.

For the internal energy, when we analyze the results, it is obvious that when the internal energy of the barrier wall decreases, this shows that the barrier wall has low resistance against blast loads, and hence, the pressure behind the barrier wall increases. On the contrary, when the internal energy of the barrier wall increases, this shows that the barrier wall has high resistance against blast loads; hence, the pressure behind the barrier wall decreases.

Conclusion

The current study investigates the response of different geometrical configurations of concrete wall barrier against blast waves and a non-linear 3d numerical model is used to model the proposed configuration. The effect of changing the structural configuration of the wall barrier is examined. The following conclusions were concluded:

1. The numerical model presented has a good agreement with the experimental work in the validation; hence, it can be used for parametric studies.
2. After comparing the different structural configurations proposed in our study, the best configuration for mitigation of blast hazards is using convex barrier walls facing the pressure wave as shown by model CCXW-60 which gave the best performance for the protection of the area behind the wall barrier where the pressure for gauge 7 behind the barrier wall for the model CCXW-60 was lower by 23.4% than the pressure measured for the concave wall (CCVW-60) with the same angle of curvature and was lower by 56% than the pressure measured for the flat wall (TFBW).
3. The convex barrier walls have the best performance in lowering the pressure affecting the wall which will consequently affect the fragments ejecting from the wall as the pressure measured on the front face in the convex walls is lower than the concave walls with an average percentage of 63.2% and lower than the flat wall with an average percentage of 66.25%. While for the back face, the pressure measured of the convex walls is lower than the concave walls with an average percentage of 45.7% and lower than the flat wall with an average percentage of 65.85%.
4. Moreover, it is also concluded that varying the angle of curvature has a notable influence on the effect of explosion on the wall barrier and the area protected by the barrier where the pressure measured behind the convex wall with 60° angle of curvature is lower by 59.7% than the pressure measured behind the convex wall with 70° angle of curvature and is lower by 47.68% than the pressure measured behind the convex wall with 50° angle of curvature. The current work proves that the response of the curvature configuration concept is much better than the flat configuration under the effect of the blast waves.
5. The internal energy of barrier walls were measured and showed that the barrier wall with the highest internal energy has the most resistance to blast loads and vice versa.

References

Aghdamy S, Wu C, Griffith M (2013) Simulation of retrofitted unreinforced concrete masonry unit walls under blast loading. Int J Protect Struct 4:21–44

Alsubaei FCF (2015) Performance of protective perimeter walls subjected to explosions in reducing the blast resultants on buildings. Phd thesis, the University of Western Ontario

Autodyn A (2005) Theory manual revision 4.3. Century Dynamics, Concord

Azmi M, Kolahchi R, Bidgoli MR (2019) Dynamic analysis of concrete column reinforced with Sio (2) nanoparticles subjected to blast load. Adv Concrete Construct 7:51–63

Baker WE, Cox P, Kulesz J, Strehlow R, Westine P (2012) Explosion hazards and evaluation, vol 5. Elsevier, Oxford

Ben-Dor G, Igra O, Elperin T (2000) Handbook of shock waves, vol 3. Elsevier, Oxford

Berger S, Ben-Dor G, Sadot O (2015) Experimental and numerical investigations of shock-wave attenuation by geometrical means: a single barrier configuration. Eur J Mech B Fluids 50:60–70

Chaudhuri A, Hadjadj A, Sadot O, Ben-Dor G (2013) Numerical study of shock-wave mitigation through matrices of solid obstacles. Shock Waves 23:91–101

Connors MJ (2014) Design of a multifunctional biomineralized armor system: the shell of chitons. Massachusetts Institute of Technology, Cambridge

Goel MD, Matsagar VA (2013) Blast-resistant design of structures. Pract Period Struct Des Construct 19:04014007

Hajek R, Foglar M, Fladr J (2016) Influence of barrier material and barrier shape on blast wave mitigation. Constr Build Mater 120:54–64

Hetherington J, Smith P (2014) Blast and ballistic loading of structures. CRC, Oxford

Hinman E, Engineers PHC (2011) Blast safety of the building envelope. Whole Building Design Guide 2011

Igra O, Wu X, Falcovitz J, Meguro T, Takayama K, Heilig W (2001) Experimental and theoretical study of shock wave propagation through double-bend ducts. J Fluid Mech 437:255–282

Li G-Q, Yang T-C, Chen S-W (2009) Behavior and simplified analysis of steel-concrete composite beams subjected to localized blast loading. Struct Eng Mech 32:337–350

Lu Y, Wang Z, Chong K (2005) A comparative study of buried structure in soil subjected to blast load using 2D and 3D numerical simulations. Soil Dyn Earthq Eng 25:275–288

Luccioni B, Ambrosini R (2010) Numerical assessment of blast effects scaling procedures. Mecanica Computacional 29:1161–1179

Mizukaki T (2007) AUTODYN electronic document Library AUTODYN electronic document Library, 1997. J Vis 10:91–98

Nam J-W, Yoon I-S, Yi S-T (2016) Numerical evaluation of FRP composite retrofitted reinforced concrete wall subjected to blast load. Comput Concrete 17:215–225

Nurick G, Gelman M, Marshall N (1996) Tearing of blast loaded plates with clamped boundary conditions. Int J Impact Eng 18:803–827

Nurick G, Chung Kim Yuen S, Jacob N, Verster W, Bwalya D, Vara A (2006) Response of quadrangular mild-steel plates to large explosive load. In: Second international conference on design analysis of protective structures (DAPS), 2006. Nanyang Technological University Singapore, pp 30–44

Porter MM, Novitskaya E, Castro-Ceseña AB, Meyers MA, McKittrick J (2013) Highly deformable bones: unusual deformation mechanisms of seahorse armor. Acta Biomater 9:6763–6770

Remennikov AM, Rose TA (2007) Predicting the effectiveness of blast wall barriers using neural networks. Int J Impact Eng 34:1907–1923

Riedel W, Thoma K, Hiermaier S, Schmolinske E (1999) Penetration of reinforced concrete by BETA-B-500 numerical analysis using a new macroscopic concrete model for hydrocodes. In: Proceedings of the 9th international symposium on the effects of munitions with structures, 1999. Berlin-Strausberg, Germany

Riedel W, Kawai N, Kondo K-i (2009) Numerical assessment for impact strength measurements in concrete materials. Int J Impact Eng 36:283–293

Rogers GFC, Mayhew YR (1995) Thermodynamic and transport properties of fluids. Blackwell, Oxford

Rong CPC, Thong CSS (2015) Learning from Mother Nature: 'Biomimicry' for the next-generation armed forces. Aust Defence Force J 197:51

Rouse NT (2010) The mitigation effects of a barrier wall on blast wave pressures

Sandhu IS, Sharma A, Singh MK, Kumari R, Alegaonkar PS, Saroha D (2017) Study of blast wave pressure modification through rubber foam. Proced Eng 173:570–576

Smith P, Rose T, Saotonglang E, CONWEP (1999) Clearing of blast waves from building facades. Proc Inst Civ Eng Struct Build 134:193–199

Tiwari AK, Tiwary AK, Dhiman A (2016) Analysis of concrete wall under blast loading. Int J Comput Appl 975:8887

Wang W, Zhang D, Lu F, Liu R (2013) A new SDOF method of one-way reinforced concrete slab under non-uniform blast loading. Struct Eng Mech 46:595–613

Wilson JO (2008) A systematic approach to bio-inspired conceptual design. Georgia Institute of Technology, Georgia

Wu C (2012) Research development on protection of structures against blast loading at University of Adelaide. Aust J Struct Eng 13:97–109

Wu C, Huang L, Oehlers DJ (2010) Blast testing of aluminum foam-protected reinforced concrete slabs. J Perform Construct Facil 25:464–474

Xia Y, Wu C, Zhang F, Li Z-X, Bennett T (2014) Numerical analysis of foam-protected RC members under blast loads. Int J Protect Struct 5:367–390

Yusof MA, Rosdi RN, Nor NM, Ismail A, Yahya MA, Peng NC (2014) Simulation of reinforced concrete blast wall subjected to air blast loading. J Asian Sci Res 4:522–533

Zhou X, Hao H (2008) Prediction of airblast loads on structures behind a protective barrier. Int J Impact Eng 35:363–375